Chemosphere 339 (2023) 139340

Contents lists available at ScienceDirect

Chemosphere

journal homepage: www.elsevier.com/locate/chemosphere

Boron-based magnesium diboride nanosheets preparation and tested for antimicrobial properties for PES membrane

Ridvan Kucukosman [a], Zelal Isik [b], Kasim Ocakoglu [a], Nadir Dizge [b], Sadin Özdemir [c], M. Serkan Yalçın [c], Prabhakar Sharma [d], Deepanraj Balakrishnan [e,*]

[a] Department of Engineering Fundamental Sciences, Tarsus University, Faculty of Engineering, Tarsus, 33400, Turkey
[b] Department of Environmental Engineering, Mersin University, Mersin, 33343, Turkey
[c] Technical Science Vocational School, Mersin University, Mersin, 33343, Turkey
[d] Department of Mechanical Engineering, Delhi Skill and Entrepreneurship University, New Delhi, India
[e] College of Engineering, Prince Mohammad Bin Fahd University, Al-Khobar, 31952, Saudi Arabia

HIGHLIGHTS

- Boron-based magnesium diboride nanosheets were prepared.
- MgB_2 nanosheets were screened for various biological and antibiofilm activities.
- The antibiofilm activity of MgB_2 nanosheets against *S. aureus* and *P. aeruginosa* was observed to be satisfactory.
- PES membrane was prepared by blending of MgB_2 nanosheets.

GRAPHICAL ABSTRACT

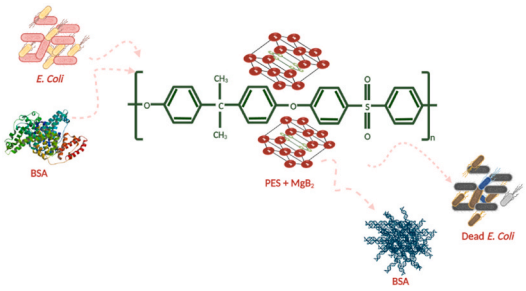

ARTICLE INFO

Handling editor Elena Niculina Niculina Dragoi

Keywords:
Magnesium diboride
MgB_2 nanosheets
Composite PES membrane
BSA separation
E. coli removal

ABSTRACT

Antimicrobial resistance to antibiotics for current bacterial infection treatments is a medical problem. 2D nanoparticles, which can be used as both antibiotic carriers and direct antibacterial agents due to their large surface areas and direct contact with the cell membrane, are important alternatives in solving this problem. This study focuses on the effects of a new generation borophene derivative obtained from MgB_2 particles on the antimicrobial activity of polyethersulfone membranes. MgB_2 nanosheets were created by mechanically separating magnesium diboride (MgB_2) particles into layers. The samples were microstructurally characterized using SEM, HR-TEM, and XRD methods. MgB_2 nanosheets were screened for various biological activities such as antioxidant, DNA nuclease, antimicrobial, microbial cell viability inhibition, and antibiofilm activities. The antioxidant activity of nanosheets was 75.24 ± 4.15% at 200 mg/L. Plasmid DNA was entirely degraded at 125 and 250 mg/L nanosheet concentrations. MgB_2 nanosheets exhibited a potential antimicrobial effect against tested strains. The cell viability inhibitory effect of the MgB_2 nanosheets was 99.7 ± 5.78%, 99.89 ± 6.02%, and 100 ± 5.84% at 12.5 mg/L, 25 mg/L, and 50 mg/L, respectively. The antibiofilm activity of MgB_2 nanosheets against *S. aureus* and *P. aeruginosa* was observed to be satisfactory. Furthermore, a polyethersulfone (PES) membrane was prepared by blending MgB_2 nanosheets from 0.5 wt to 2.0 wt %. Pristine PES membrane also has shown the lowest steady-state fluxes at 30.1 ± 2.1 and 56.6 L/m^2h for BSA and *E. coli*, respectively. With the

* Corresponding author.
E-mail address: babudeepan@gmail.com (D. Balakrishnan).

https://doi.org/10.1016/j.chemosphere.2023.139340
Received 18 March 2023; Received in revised form 16 June 2023; Accepted 24 June 2023
Available online 26 June 2023

increase of MgB_2 nanosheets amount from 0.5 to 2.0 wt%, steady-state fluxes increased from 32.3 ± 2.5 to 42.0 ± 1.0 and from 15.6 ± 0.7 to 24.1 ± 0.8 L/m^2h, respectively for BSA and *E. coli*. *E. coli* elimination performance of PES membrane coated with MgB_2 nanosheets at different rates and the membrane filtration procedure was obtained from 96% to 100%. The results depicted that BSA and *E. coli* rejection efficiencies of MgB_2 nanosheets blended PES membranes increased when compared to pristine PES membranes.

1. Introduction

Water scarcity and pollution have become a worldwide concern due to increasing urbanization, industry, and technological advancements, posing a danger to the entire ecosystem and harming people's health (Jessop et al., 2013). Membrane technology is still the most effective treatment and water recovery system, with the best prospects in wastewater applications, as compared to other physical, chemical, physicochemical, or biological treatment systems (Scheifers et al., 2017). Sadly, the most significant disadvantage of membrane-based separation is membrane fouling, which decreases the permeation flux and hence raises operational and maintenance costs (Li et al., 2015). Therefore, the membrane surface needs to be modified in various ways to prevent the fouling mechanism.

Due to their resilience in the face of challenging process conditions and universal acceptance as materials that are safe for both people and animals, inorganic materials including metal, metal oxides, and nanoparticles have gained increased attention in recent years (Mubeen et al., 2021). The inorganic nanoparticles and their derivatives have effective biocidal effects (Dizaj et al., 2014). Inorganic antibacterial agents interact directly with the membrane of the microbial cell, which causes physical harm to the membrane. Thus, it can create oxidative stress on the microbial cell and completely destroy the cell. Due to their extensive surface area, enhanced mechanical strength, distinctive physiochemical characteristics, and high biocompatibility, graphene, and hexagonal boron nitride are known to have potent antibacterial capabilities (Deshmukh et al., 2020; Krishnamoorthy et al., 2012). Recently, in light of this information, current research and development is directed toward the use of new antimicrobial agents based on two-dimensional (2D) materials. However, the number of reported studies for borophene derivatives is very few and only the β-rhombohedral crystalline borophene derivative has been investigated, except for boron nitride. It has been found that β-rhombohedral crystalline borophene nanosheets have inhibitory activity against many medically serious bacterial and fungal pathogenic microorganisms such as *Staphylococcus aureus*, *Pseudomonas aureginosa*, *Escherichia coli*, *Candida albicans*, and *Aspergillus brasilliensis* (Taşaltın et al., 2022).

The characteristics of boron, including its low density and high strength, high heating value, and capacity to absorb neutrons, make it a desirable material for use in a range of industries, from surface engineering to energy (Efeoğlu et al., 2019; Liang et al., 2017). To fully exploit these properties of boron, interest in the creation of 2D planar structures has grown in nanoscience and technology. The manufacturability of semi-planar boron-based materials and 2D borophene sheets was investigated by computational modeling studies. Reported studies with first principle calculations have shown that boron nanolayers can be deposited on metals (Cu, Ag, and Au) and metal boride substrates such as MgB_2 and TiB_2 (Zhang et al., 2015). Although many theoretical studies on boron forms have been conducted, experimental research on the production of 2D boron derivates is still in its early stages. In recent years, the experimental production of boron layers has been announced by the thermal decomposition of diborane (Xu et al., 2015), the decomposition of metal boride precursors at high temperatures (Patel et al., 2015), on metallic substrates under ultra-high vacuum pressure (Mannix et al., 2015), and by techniques such as chemical vapor deposition (CVD) involving different boron sources (Tai et al., 2015). Bottom-up vapor phase approaches are used in these boron planarization studies. Even though the 2D forms achieved from these methods are stable, the boron atoms in these layered structures are not arranged in a honeycomb structure. The structures are built up of groups of B36, B12, or B7 boron atoms organized in 2D.

MgB_2, a compound composed of Mg cations and hexagonal boron plates, and amorphous boron particles were used in the top-down approach for borophene 2D sheets (Gunda et al., 2018; Li et al., 2018; Nishino et al., 2017). In applications where MgB_2 is the primary material, 2D MgB_2 nanosheets were created by ultrasonication a room-temperature mixture of water and MgB_2. As a result of the reaction of MgB_2 and water, the resulting Mg-deficient hydroxyl functional boron nanosheets are grouped as one of the stabilized 2D borophene sheets. Exfoliation of MgB_2 in liquid media is the most effective and efficient way to produce 2D borophene sheets with a top-down approach.

Boron and its derivatives are known to be important alternatives for antimicrobial and biocompatibility applications. However, the production of boron-based NPs with 2D structure and functional groups on the surface is difficult and the variety is limited. In this regard, MgB_2 nanosheets seem to be an important alternative for antimicrobial applications due to their efficient and easy production and deserve research interest in this field. In this study, MgB_2 nanosheets obtained by exfoliation of MgB_2 particles were doped into the structure of PES membranes, and the antimicrobial properties of the membranes were investigated. MgB_2 nanosheets were prepared by ultrasonication of MgB_2 in pure water. Structural characterizations of boron-based magnesium diboride nanosheets were performed by SEM, HR-TEM, and XRD techniques. MgB_2 nanosheets were incorporated into a polyethersulfone (PES) membrane to generate a composite membrane with improved antifouling and permeability against bovine serum albumin (BSA) and *E. coli*, as confirmed by characterization methods. To the best of our knowledge, no studies on PES membranes modified with MgB_2 nanosheets have been reported in the literature.

2. Materials and methods

2.1. Chemicals

MgB_2 particles with a diameter of 28–35 μm were purchased from Pavezyum Technical Ceramic. Polyethersulfone with a molecular weight of 58,000 g/mol was kindly obtained by the BASF Company (Germany). Dimethyl sulfoxide (DMSO) and bovine serum albumin (BSA, Mw: 66,000 g/mol) were supplied by Merck Company (Germany). Those chemicals were of analytical grade, and distilled water was obtained using a two-stage Millipore Direct-Q3UV purification system.

2.2. Synthesis and characterization of MgB_2 nanosheets

MgB_2 nanosheets were produced by ultrasonication of MgB_2 particles in pure water (Gunda et al., 2018; Nishino et al., 2017). MgB_2 (1 g) powder was sonicated for two days in 300 mL of deionized water. Initially, the black-colored mixture turned into a heterogeneous mixture with gray particles color and a yellow liquid medium. The particles were removed from the mixture, and the yellow supernatant was allowed to crystallize for four days. The solution, which had a transparent appearance, was heated to 90 °C, and pure water was removed. The white precipitated crystals were collected and 1.5 g of product was obtained. In Fig. 1, the main steps of the production process are presented schematically.

Surface morphologies of MgB_2 nanosheets were determined by FEI-

Quanta 650 field emission scanning electron microscope (SEM). High-resolution transmission electron microscopy (HR-TEM) pictures were obtained using an FEI TALOS F200S TEM with a 200 kV accelerating voltage. Phase structures were analyzed with a Cu-Kα sourced Panalytical Empyrean X-Ray diffractometer (XRD) at a wavelength of λ = 1.54 A°. Measurements were taken at 2θ = 5°–90° and 0.01313° steps at 300 K room temperature.

2.3. Preparation of PES membranes with pristine and MgB_2 nanosheets

The pristine and MgB_2 nanosheets blended composite membranes were created using the phase inversion method (Fig. 2). The PES beads were oven-dried at 80 °C for 2 h before use. To make functionalized membranes, different ratios of MgB_2 nanosheets (0.5, 1.0, 2.0%wt.) were added to NMP solvent and dispersed for 15 min using an ultrasonication bath before adding PES beads (15%wt.) to this solution. The solution was vigorously mixed at 60 °C for 6 h, then at ambient temperature up overnight before being ultrasonicated for 20 min to obtain a clear homogeneous solution and eliminate air bubbles from the casting solutions. When all bubbles were removed, casting solutions consisting of MgB_2 nanosheets were spread on a glass plate with a casting knife gap setting of 200 μm at a speed of 100 mm/s. Following that, the glass plates were immersed in deionized water to achieve polymer sedimentation. The membranes were removed from the water bath, and to ensure complete phase inversion placed in fresh purified water for at least 1 day after manufacture (M'barek et al., 2022). All membranes were tested at 5 bar with distilled water before the experiments.

The surface microstructure of the pristine PES and MgB_2 nanosheets addition PES membranes was examined using SEM (SEM, Gemini Zeiss Supra 55). The membranes were coated with a gold layer after drying at room temperature. The dead-end filtration module with a 14.6 cm^2 active area was used to test the filtration performance of the manufactured membranes. The filtration experiments were carried out at room temperature and 1 bar of pressure. To test the efficiency of membranes, the dead-end filtration system was separately loaded with 100 mg/L of BSA solution (50 mM of Phosphate Buffer Solution, pH 7.4) and 1×10^8 CFU/mL of *E. coli* solution. BSA solution was prepared to prevent protein denaturation. All solutions were filtered for 120 min at 1 bar. The Lowry method was used to determine the BSA concentration of the feed (C_f) and permeate (C_p).

2.4. DPPH scavenging activity

The antioxidant capability of MgB_2 nanosheets was investigated using the scavenging of stable 2,2-diphenyl-1-picrylhydrazyl (DPPH) free radicals. The stock solution of MgB_2 nanosheets and references (ascorbic acid and Trolox) were diluted in various concentrations as 12.5, 25, 50,100, and 200 mg/L. A 250 μL sample was added to 1000 μL methanolic DPPH solution and mixed thoroughly. As a control, the assay mixture without MgB_2 nanosheets was also tested. The test tubes were then held at 25 °C in the dark for 30 min. In the presence of a radical scavenger, the dark purple color of the DPPH solution is removed and changes to pale yellow. At 517 nm, absorbance was then measured. In order to calculate the percentage of inhibitory activity, formula (1) was used:

$$\text{DPPH scavenging inhibition\%} : \left[\left(A_{control} - A_{sample}\right) / \ A_{control}\right] \text{x } 100 \quad (1)$$

2.5. DNA cleavage assay

The DNA nuclease activity of MgB_2 nanosheets was investigated against pBR322 supercoiled plasmid DNA using the agarose gel electrophoresis technique. The DNA was mixed with various concentrations of MgB_2 nanosheets and incubated at 37 °C for 90 min. Untreated DNA was applied as the control with DMSO at a final concentration of 1%. The nanoparticles samples were then loaded onto a 1.0% agarose gel and stained with EthBr in a Tris-acetic acid-EDTA buffer. For 1.5 h, the samples were tested at 100 V. Finally, the electrophoresis bands were visualized and photographed using a UV illuminator.

2.6. Antimicrobial efficiency

The antimicrobial efficacy of MgB_2 nanosheets was examined against *Enterococcus faecalis* (ATCC 29212), *Enterococcus hirae* (ATCC 10541), *Staphylococcus aureus* (ATCC 25923), *Legionella pneumophila* subsp. *pneumophila* (ATCC 33152), *Escherichia coli* (ATCC 25922), *Pseudomonas aeruginosa* (ATCC 27853), *Candida tropicalis* (ATCC 750) and *Candida albicans*. In our lab, we had all the microbiological cultures available. Using the standard broth microdilution method, the minimum inhibitory concentrations (MICs) of MgB_2 nanosheets were assessed. To activate the microbiological cultures, microbes were inoculated in a liquid medium (Nutrient Broth, NB) and grown overnight at 37 °C in a constant mixer. The test microorganisms were then diluted with NB to a concentration of 10^8–10^9 CFU/mL and added to the medium-containing microplate wells. The tested nanoparticle was added to the first well of 1024 mg/L and diluted in the remaining wells. In order to incubate, 96 well microplates were kept at 37 °C for one day on the shaker. Using a microplate reader, the microplates were recorded at 600 nm to determine the MIC values.

2.7. Microbial cell viability inhibition test

The cell viability inhibiting capacity of MgB_2 nanosheets was investigated against *E. coli* (ATCC 10536) as a model bacterial strain. The cells were collected using a centrifuge at 5500 rpm for 7 min after *E. coli* cultivation. The bacterial cell pellet was washed in a sterile NaCl solution to remove the residual medium. In 10 mL of NaCl solution, the clean bacterial cell pellet was suspended. At 37 °C for 90 min, *E. coli* was treated with/without 12.5, 25, and 50 mg/L MgB_2 nanosheets. Following various NaCI dilution ratios, the mixtures were inoculated onto NB agar and incubated for 1 day at 37 °C. The number of colonies was then determined, and the following equation (2) was used to determine the cell viability inhibition.

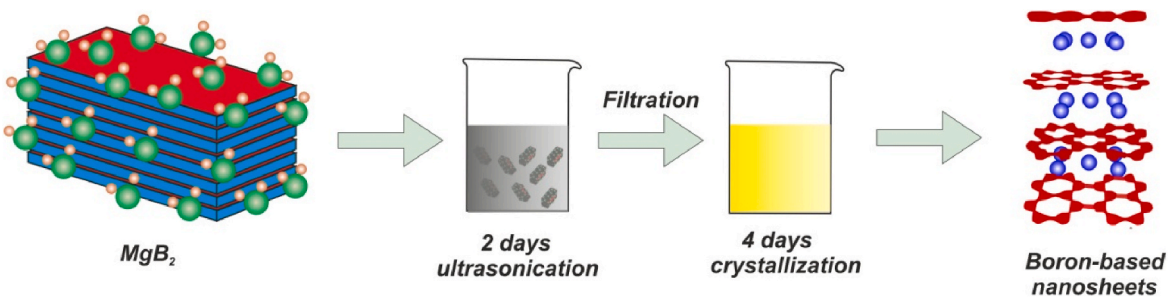

Fig. 1. The main steps of the MgB_2 nanosheet production process.

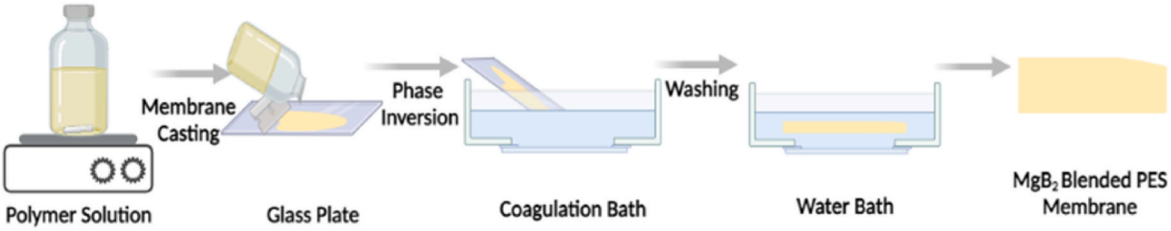

Fig. 2. Schematic presentation of the MgB_2 blended PES membrane production process.

$$\text{Microbial Cell viability inhibition}(\%) : \left[\left(A_{control} - A_{sample}\right) / \ A_{control}\right] x\ 100 \quad (2)$$

2.8. Biofilm inhibition activity

The biofilm inhibitory capacity of MgB_2 nanosheets was evaluated against *P. aeruginosa* (ATCC 27853) and *S. aureus* (ATCC 25923). After inoculating bacterial cells into the wells with varying doses of MgB_2 nanosheets, the microplates were incubated at 37 °C for three days. The wells were then emptied, and the adherent cells in the microplate wells were gently washed with pure water. After drying, adherent cells were stained with crystal violet. The dye was poured off after 1 h, and the microplate wells were washed with pure water. Crystal violet penetrating the biofilm was recovered using ethanol and its absorbance was measured at a wavelength of 595 nm. The well without MgB_2 nanosheets was used as a control. In order to determine the effectiveness of MgB_2 nanosheets on the inhibition of biofilm-forming, the below equation (3) was used.

$$BiofilmInhibition(\%) = \left(\frac{Abs(control) - Abs(sample)}{Abs(control)}\right) \times 100 \quad (3)$$

2.9. E. coli removal and E. coli filtering process effectiveness of PES membrane coated with MgB_2 nanosheets

E. coli removal and *E. coli* filtration process improvement of PES membrane mixed with MgB_2 nanosheets were investigated according to the literature (Saleh et al., 2021). *E. coli* removal performance was evaluated using the equation in subsection ''Microbial cell viability inhibition activity''.

3. Results and discussion

3.1. Characterization of MgB_2 nanosheets

SEM images of the surface morphology of boron-based MgB_2 nanosheets are presented in Fig. 3a and b. HR-TEM image of MgB_2 nanosheets is presented in Fig. 3c, and the XRD diffraction pattern is presented in Fig. 3d. MgB_2 nanosheets contain curving sections, demonstrating the resilient nature of the sheets (Nishino et al., 2017). Based on the cross-section of the sheets in Fig. 3b, the thickness of the layers can be estimated to be 30 nm. Fig. 3c reveals the uniform long 2D nanosheet structure. The XRD reflections showed clear diffraction peaks. The distinct XRD peaks observed at 12.6° (0.702 nm) and 36.7° (0.245 nm) and the peak observed at 60.2° (0.156 nm) differ from those observed in MgB_2 (Nishino et al., 2017). The peak at 12.6° is most likely due to the sheets' layering periodicity. Such characteristic peaks can be seen in 2D layered materials such as graphite intercalated compounds. The source of the other peaks is thought to be due to the phases formed on the sheets. Peaks at 36.7° (101) and 60.2° (210) indicate the presence of the $Mg(OH)_2$ phase.

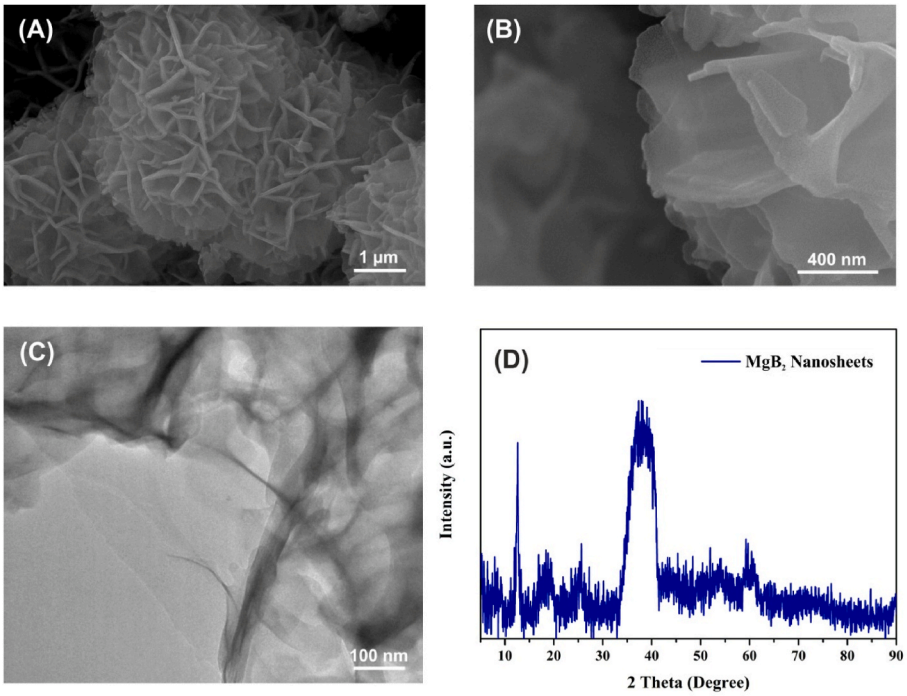

Fig. 3. (A,B) SEM image of the surface morphology, **(C)** HR-TEM micrography, and **(D)** XRD diffraction pattern of MgB_2 nanosheets.

3.2. Characterization of MgB_2 nanosheets blended composite membrane

SEM images of the prepared pristine and composite membranes are shown in Fig. 4. There was a smooth surface on the pristine membrane (Fig. 4A). SEM images indicated that the uniform long 2D nanosheet structures were also observed for MgB_2 nanosheets blended composite membranes (Fig. 4B–D). When the amount of boron-based MgB_2 nanosheets increased from 0.5% to 2.0% on the surface, agglomeration also increased. The energy dispersive spectrometry (EDS) mapping revealed that MgB_2 nanosheets were widely distributed within the PES membrane structure (Fig. 5).

3.3. Antioxidant activity by DPPH scavenging assay technique

Because of its low cost, simplicity of use, and effectiveness, the DPPH free radical scavenging assay is frequently used as a fundamental screening technique to evaluate the anti-radical activity of different substances (Bajpai et al., 2017). To determine the scavenging ability of MgB_2 nanosheets, it was applied at different concentrations of 12.5, 25, 50, 100, and 200 mg/L. Fig. 6 depicts the data comparing the percentage free radical scavenging capacity of MgB_2 nanosheets with ascorbic acid and Trolox as standards. At a concentration of 12.5 mg/L, MgB_2 nanosheets demonstrated a minimum of 51.07 ± 2.86% DPPH scavenging activity, while ascorbic acid and Trolox demonstrated 84.12 ± 5.21 and 86.39 ± 5.09, respectively. The NPs showed a maximum scavenging activity of 75.24 ± 4.15%, but ascorbic acid and Trolox showed 100 ± 7.25% activity whenever the concentration was raised to 200 mg/L. MgB_2 nanosheets exhibited 51.07 ± 2.86%, 54.38 ± 2.91%, 59.84 ± 3.34%, 68.22 ± 3.58%, and 75.24 ± 4.15% scavenging activity at doses of 12.5, 25, 50, 100, and 200 mg/L respectively. It is clearly seen that the radical scavenging property of the nanoparticle varies in a dose-dependent manner. Dobrucka (2018) synthesized MgO NPs using a herbal extract and reported that they showed efficient antioxidant activity (Dobrucka, 2018). John Sushma et al. (2016) produced biologically synthesized MgO NPs has 65% DPPH scavenging activity (John Sushma et al., 2016). They stated that the bioactive components in the *C. ternatea* extract may be the cause of this greatest inhibition of MgO NPs. We can infer from our findings that MgB_2 nanosheets have a potent anti-radical action.

3.4. DNA cleavage activity

In order to evaluate the chemical nuclease activities of the MgB_2 nanosheets, supercoiled plasmid DNA as a substrate was used. This ability of any compound or molecule investigated for DNA nuclease activity is assessed by causing the supercoiled circular form of pBR322 plasmid DNA to relax into the nicked circular form and the linear form. The DNA fragmentation image of this study is presented in Fig. 7. Supercoiled circular DNA was converted to nicked circular DNA at 62.5 mg/L concentrations of MgB_2 nanosheets, while at 125 and 250 mg/L concentrations supercoiled DNA was completely cleaved. However, the untreated DNA used for control was not cleaved The pathogenic microorganisms in wastewater cause some infections and diseases like viral, bacterial, fungal, and protozoan (Olaolu et al., 2014). According to our findings, MgB_2 nanosheets can cleave the genomes of pathogenic microorganisms to prevent them from microbial growth. Khalid et al. (2023) prepared TiO_2+ZnO nanoparticles using co-precipitation wet chemical method to generate highly reactive oxygen species (ROS). It has been reported that the modified band gap controls the energy of the excited electrons and produces a higher rate of ROS. The ROS distracted mitochondria membrane and DNA causing death of cancer cells. In another study, nickel nanoparticles (Ni-NPs) with a size of 56.09 ± 3.75 nm were used for reproductive toxicants for male rats (Iftikhar et al., 2023). Accumulation of Ni-NPs caused harmful reproductive destruction in male rats due to histological abnormalities such as basement membrane damage, vacuation, necrosis, loss of spermatogenic series, sloughing.

3.5. Antimicrobial activity

Significant scientific interest in creating new biocidal or disinfecting compounds to support traditional antibiotics has been raised by the development of effective remediation processes for water-borne pathogens (Dutta et al., 2013). The antibacterial properties of inorganic NPs including gold, silver, copper, ZnO, TiO_2, CuO, etc. are extremely strong (Dizaj et al., 2014). The micro-dilution method was used to assess the antimicrobial potential of MgB_2 nanosheets, and the results are summarized as MIC values in Table 1. MIC values of MgB_2 nanosheets were 8 mg/L against *E. faecalis*, 32 mg/L against *E. hirae*, 64 mg/L against *E. coli*, *S. aureus*, *C. albicans*, *C. tropicalis*, and 128 mg/L against *P. aeruginosa*, and *L. pneumophila* subsp. *pneumophila*. It was notable that

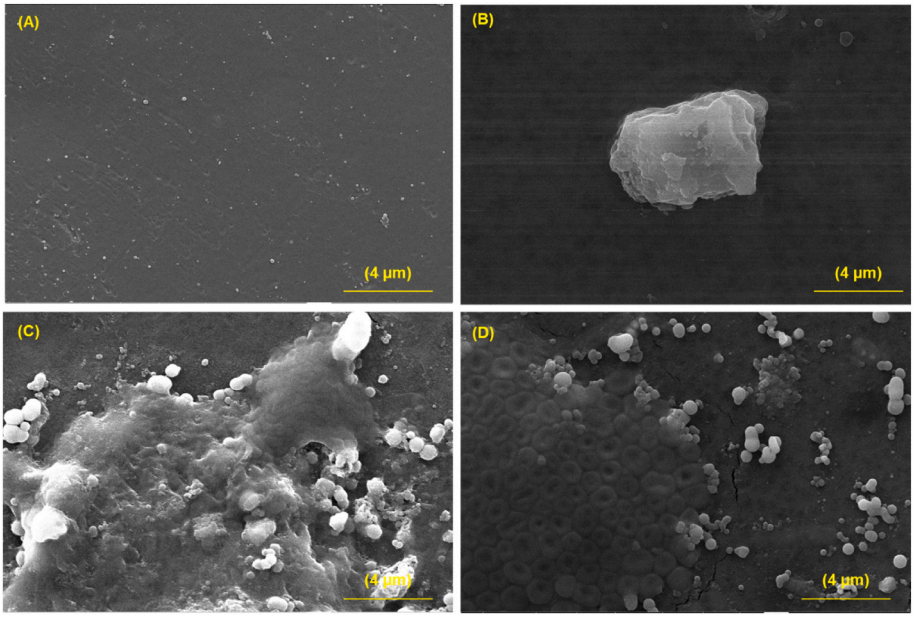

Fig. 4. SEM images for prepared MgB_2 nanosheets blended composite membranes.

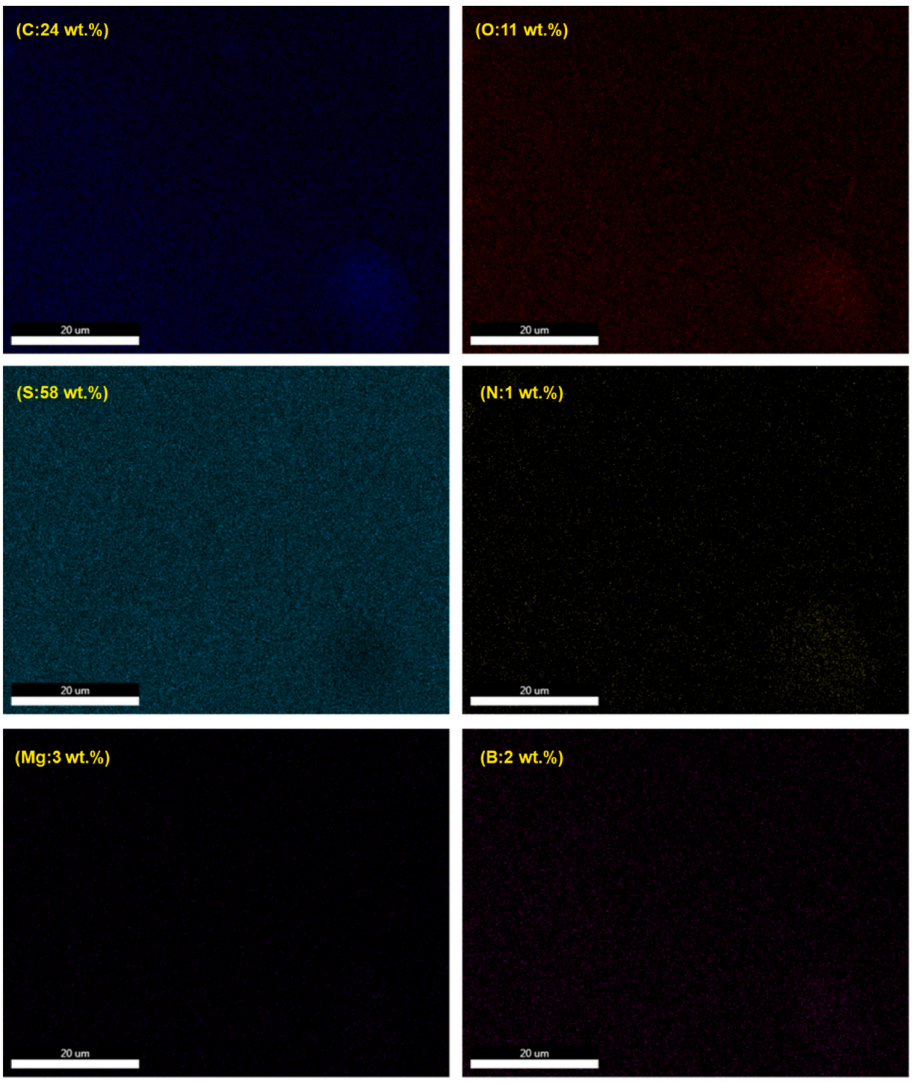

Fig. 5. EDX images for prepared MgB_2 nanosheets blended composite membranes.

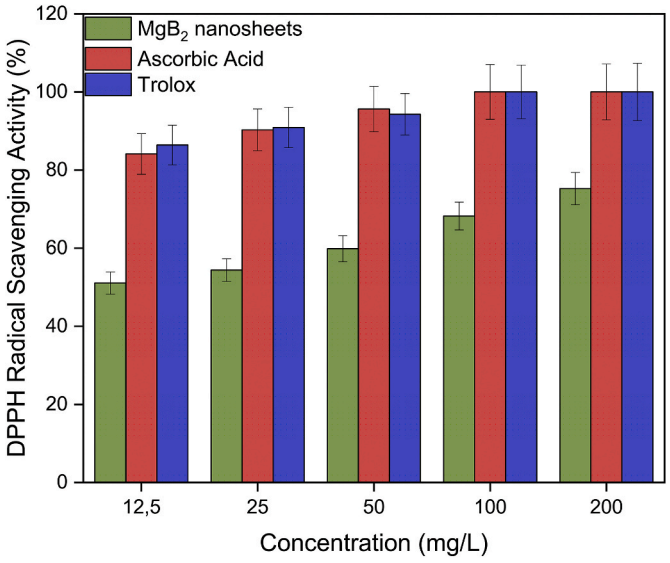

Fig. 6. Antioxidant activity of boron-based MgB_2 nanosheets.

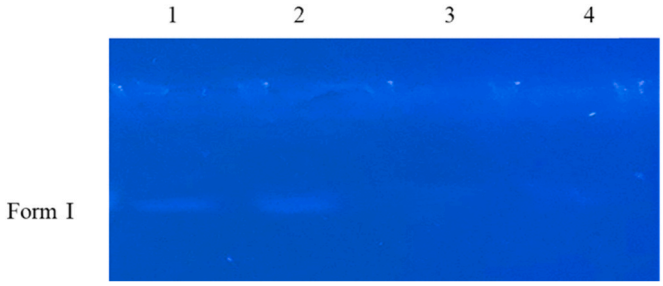

Fig. 7. DNA cleavage activity of MgB_2 nanosheets (1: Plasmid pBR322 DNA; 2: Plasmid pBR322 DNA + 62.5 mg/L MgB_2 nanosheets; 3: Plasmid pBR322 DNA + 125 mg/L MgB_2 nanosheets; 4: Plasmid pBR322 DNA + 250 MgB_2 nanosheets).

MgB_2 nanosheets exhibited more inhibitor effect against tested gram-positive bacteria such as *E. faecalis*, *E. hirae*, and *S. aureus* than the gram-negative such as *E. coli*, *P. aeruginosa*, and *L. pneumophila*. This can be explained by the difference in the cell wall structure of these bacterial species. Moreover, morphological and physicochemical characteristics such as size, shape, and positive surface charge of the nanoparticles also influence their antimicrobial properties (Seil and Webster, 2012). Pugazhendhi et al. (2019) synthesized MgO NPs using biogenic sources.

Table 1
Antimicrobial activity of boron-based MgB_2 nanosheets.

Microorganisms	MIC values (mg/L)
E. coli	64
P. aeruginosa	128
L. pneumophila subsp. *pneumophila*	128
E. hirae	32
E. faecalis	8
S. aureus	64
C. albicans	64
C. tropicalis	64

They reported MgO NPs showed potent antibacterial activity against *S. pneumonia*, *S. aureus*, *E. coli*, *P. aeruginosa*, and *A. baumannii*. The antimicrobial activity of boron nitride was investigated by Kıvanç et al. (2018). In this study, they reported nanoparticles were effective against *S. mutans* 3.3, *Candida* sp. M25. As a result, MgB_2 nanosheets can use as an antimicrobial agent after further experimental studies.

3.6. Microbial cell vitality inhibition

The effectiveness of MgB_2 nanosheets on inhibition of bacterial cell viability was evaluated using *E. coli* as a model bacteria. The percentage of *E. coli* viability inhibition activity is presented in Fig. 8. The inhibitory effect of the MgB_2 nanosheets was obtained as 99.7 ± 5.78%, 99.89 ± 6.02%, and 100 ± 5.84% at 12.5 mg/L, 25 mg/L, and 50 mg/L, respectively. In light of our findings, it can be said that MgB_2 nanosheets have a significant inhibitory impact. This impact can be attributed to large-surface-area nanoparticles covering bacterial cells, which prevents the bacteria from effectively using their resistance mechanisms since they can't reach the culture media (Wang et al., 2017a, b). Similarly, Das et al. (2018) has been synthesized MgO nanoflakes by using leaf extract of *Bauhinia purpurea* and assessed the viability of *S. aureus* cells after treatment with MgO nanoflakes (Das et al., 2018). They reported that at 1000 μg/mL of MgO nanoflakes concentration, no viable cells were detected after 8 h of incubation. The results of the subsequent research suggest that MgB_2 nanosheets may be used to prevent microbial growth.

3.7. Biofilm inhibition

P. aeruginosa and *S. aureus* are capable of generating biofilms that can withstand antibiotic treatment and result in chronic infection. Therefore, attacking biofilms is a suggested alternative way of dealing with this situation (Jasim et al., 2020). The ability to inhibit biofilm formation of MgB_2 nanosheets was investigated against *S. aureus* and *P. aeruginosa* biofilm formed in polystyrene microplate wells. The inhibition results against *S. aureus* and *P. aeruginosa* are shown in Figs. 9 and 10, respectively. Biofilm inhibition rates of MgB_2 nanosheets at concentrations of 12.5, 25, and 50 mg/L, against *S. aureus* and *P. aeruginosa*, were obtained as 69.13 ± 3.84%, 78.52 ± 4.26%, 91.27 ± 5.67% and 45.21 ± 2.43%, 53.18 ± 3.15%, 76.49 ± 4.48%, respectively. Obviously, MgB_2 nanosheets exhibited less antibiofilm effect against gram-negative *P. aeruginosa* than the gram-positive bacteria *S. aureus*. The antibiofilm activity of MgO NPs was investigated by MubarakAli et al. (2019). They indicated that most of the examined uropathogenic bacterial biofilm formations inhibited MgO NPs by more than 50%. The

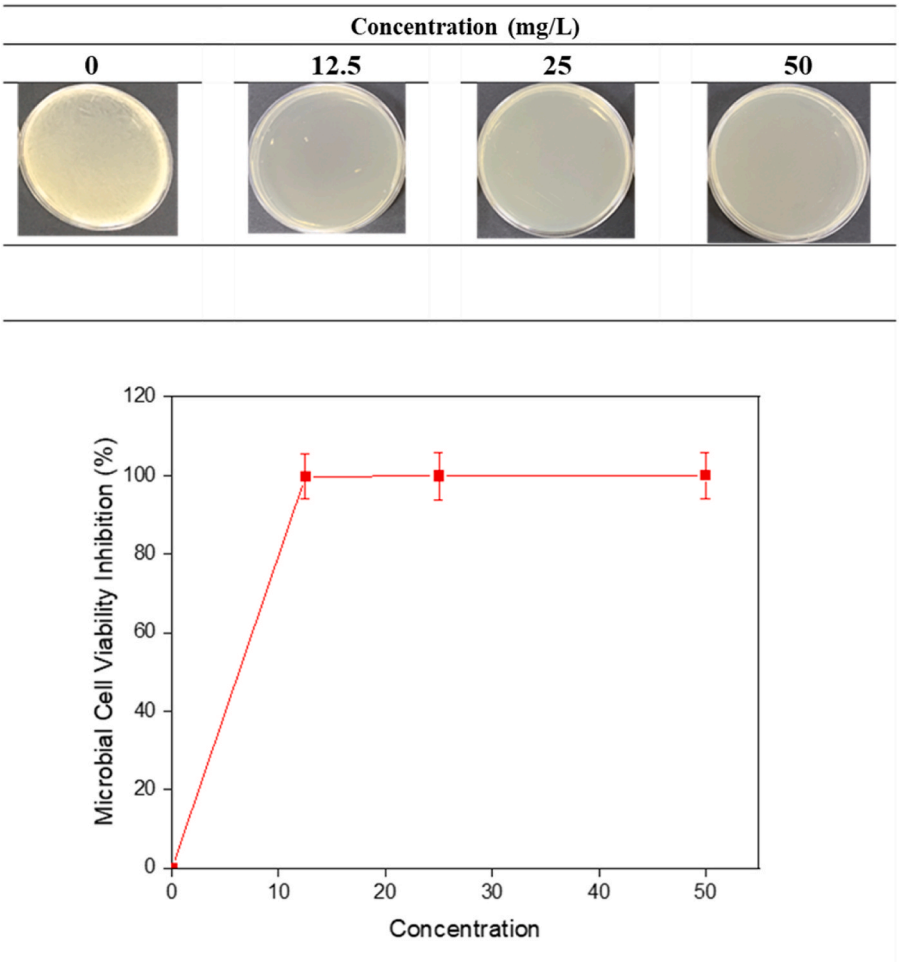

Fig. 8. Microbial cell viability inhibition of MgB_2 nanosheets.

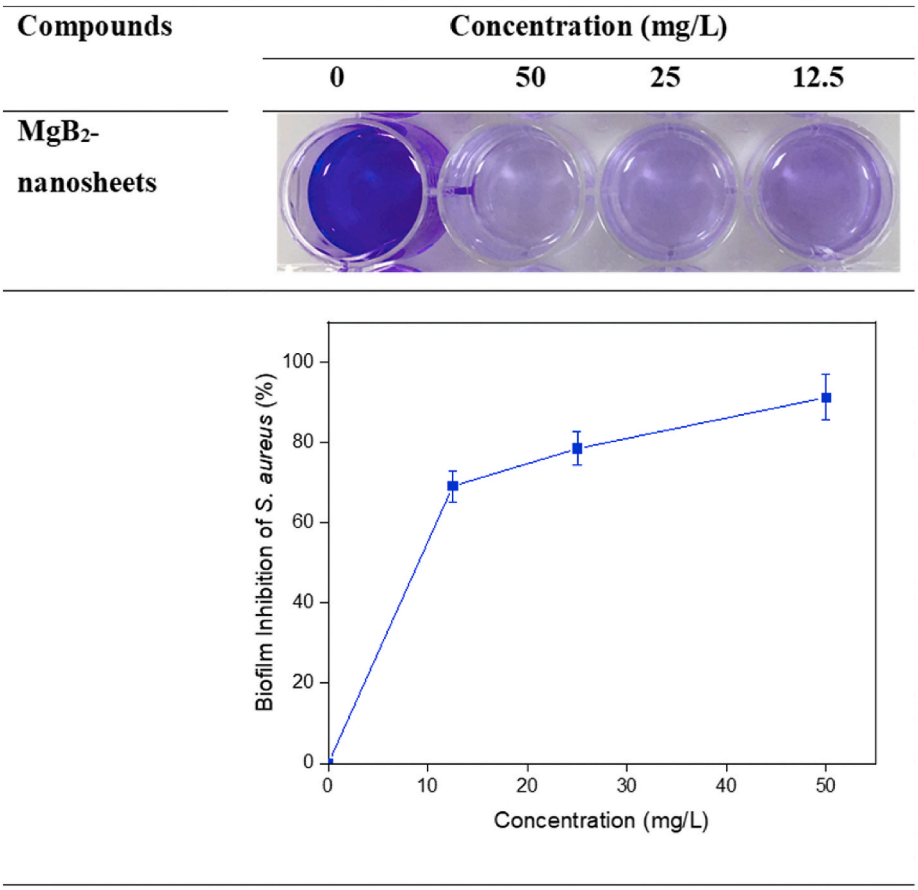

Fig. 9. Biofilm inhibition of *S. aureus* of MgB_2 nanosheets.

biofilm formation of *K. pneumoniae* was also particularly notable with an 80% inhibition rate. Kıvanç et al. (2018) reported that boron nitride nanoparticles exhibited a high antibiofilm activity on preformed biofilm, which inhibited biofilm growth of *S. mutans* ATTC 25175, *Candida* sp. M25, and *S. mutans* 33. The effect of the nanoparticle can be attributed to the inhibition of exopolysaccharides, which are mainly composed of proteins, nucleic acids, polysaccharides, and lipids, which provide biofilm formation (Di Martino, 2018). As a result, newly synthesized MgB_2 nanosheets can be used as an *anti*-biofilm agent against biofilm-forming microorganisms.

3.8. The performance of the MgB_2 nanosheets composite membranes

The prepared membranes' pure water flux (PWF) decreased from pristine PES to MgB_2 nanosheets blended PES (Fig. 11A). The decrease in hydrophilicity could explain the increase in flux from 169.7 L/m^2/h (for pristine membrane) to 275.1 L/m^2/h (for PES/MgB_2 2.00 wt% membrane). However, BSA fluxes also increased from 30.1 ± 2.1 (for pristine membrane) to 42.0 ± 1.0 L/m^2/h (for PES/MgB_2 2.00 wt% membrane) (Fig. 11B). The composite membranes' ability to remove BSA was also tested (Fig. 11C). When the amount of blended MgB_2 nanosheets increased from 0 to 2.00 wt%, BSA removal efficiency increased from 65.5 ± 2.2% to 95.5 ± 1.5%. The composite membranes' higher hydrophilicity improved BSA rejection. The porous 2D covalent organic nanosheets (CONs) membrane was prepared by Yao et al. (2020). In the study, azo-template exfoliation method was used to exfoliate covalent organic frameworks (COFs) into large-scale and few-layer nanosheets. The as-prepared nanosheets membrane showed a higher water flux (596 L m^2 h^{-1} bar^{-1}) than a graphene oxide (GO) membrane (4.3 L m^2 h^{-1} bar^{-1}). Moreover, Tp-AD-50 exhibited rejection rates as high as 98.5% (DR80), 98.3% (DR23), 82% (CR), 98% (RB), and adsorption for 88.3% (MV), due to the nano-channels perpendicular to the surface of the membrane. In addition to 2D COF nanosheets, the inherent porous g-C_3N_4 nanosheets were prepared through the assembly of partially exfoliated g-C3N4 nano sheets (Wang et al., 2017a, b). A thick g-C_3N_4 membrane (160-nm) exhibited a good water permeance of 29 L m^{-2} h^{-1} bar^{-1}, together with rejection rates of 75.5% (Rhodamine B), 87.2% (Evans Blue), 93.1% (Cytochrome C), and 99.5% (Au nanoparticles with 5 nm diameter). The mixed assembly membranes were also synthesized to improve water permeability and dye rejection. For example, hybrid GO/COF-1 nanocomposite membranes were prepared through in situ growth of COF-1 on the surface of GO nanosheets (Zhang et al., 2019). The prepared membranes presented good water permeability (310 L m^{-2} h^{-1} Mpa^{-1}) and high dye (Congo Red, Methylene Blue, Reactive Black 5, Direct Red 23, Erichrome Black T) removal efficiencies over >99%. Moreover, electrostatic interaction also played an important role for the rejection process.

In this study, the antifouling performance of the composite membranes was also investigated for *E. coli* filtration. An increase in the flux was obtained from 12.2 L/m^2/h (for pristine membrane) to 23.4 L/m^2/h (for PES/MgB_2 2.00 wt% membrane) when *E. coli* was filtrated (Fig. 12A). It can be concluded that MgB_2 nanosheets protected the composite membrane surfaces against fouling. R_{ir} values decreased from 60.5% (for pristine membrane) to 26.9% (for PES/MgB_2 2.00 wt% membrane) while R_r values increased from 20.5% (for pristine membrane) to 58.6% (for PES/MgB_2 2.00 wt% membrane) after blending of MgB_2 nanosheets (Fig. 12B). Furthermore, the FRR and R_r/R_{ir} ratios of the membranes are shown in Fig. 12C. MgB_2 nanosheets prevented irreversible *E. coli* adsorption into composite membranes in order to form a hydration layer close to the membrane surface (Russell et al., 2015). FRR values increased from 39.4% for pristine PES membrane to 73.0% for PES/MgB_2 2.00 wt% membrane (Fig. 12C). Polyvinyl alcohol

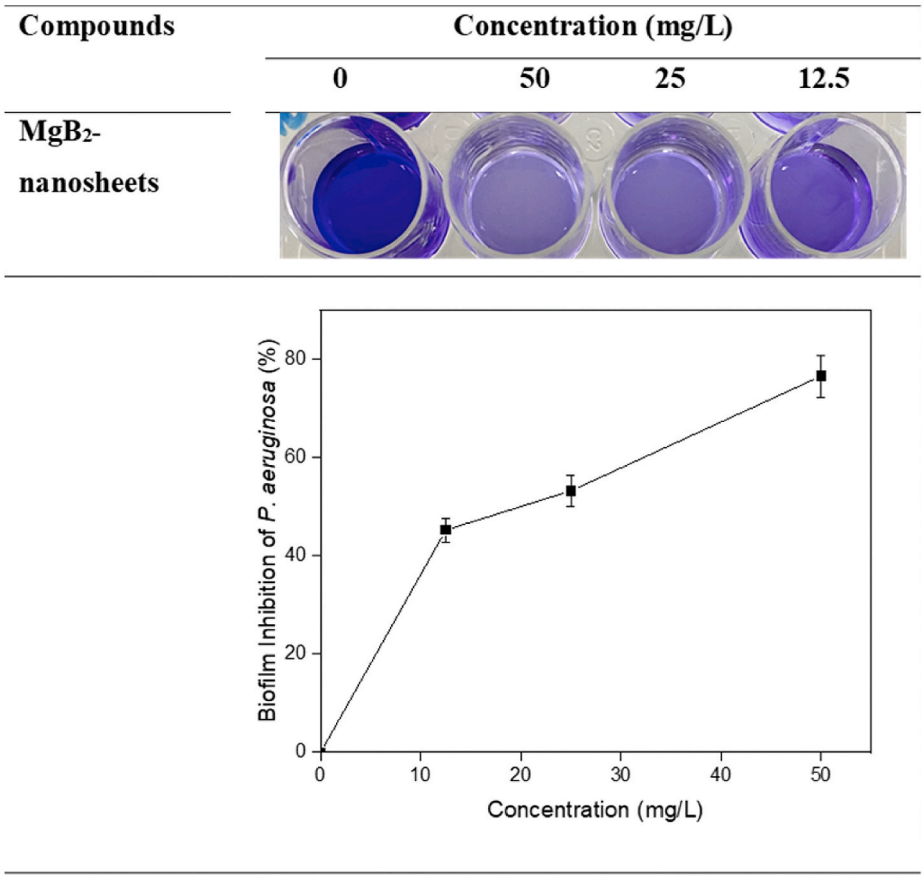

Fig. 10. Biofilm Inhibition of *P. aeruginosa* of MgB_2 nanosheets.

(PVA) and starch integrated with metal-organic frameworks (MOFs) were used to fabricate biodegradable packaging films (Khan et al., 2021). ZIF-67 and pyrolyzed ZIF-67 were doped (2–10 wt%) in a PVA/starch mixture and films were fabricated using the solution casting method. The amount of ZIF-67 in the PVA–starch blend was optimized for mechanical strength. The membranes containing pyrolyzed ZIF-67 enhanced mechanical strength of the nanocomposite membranes and the highest mechanical strength of 25 MPa was measured at 4 wt% pyrolyzed MOFs. The pyrolysis caused to increase surface area, which assisted to increase the strength of the nanocomposite films.

3.9. E. coli removal and E. coli filtering process effectiveness of PES membrane blended with MgB_2 nanosheets

Freshwater scarcity due to human activity or natural causes is seen as a growing problem. Therefore, it is necessary to focus on solutions that include diversified water resources (Mavukkandy et al., 2020). Preventing unnecessary water consumption, treatment and recovery of wastewater, desalination, and freshwater production are possible solutions. Membrane technologies used for desalination and treatment of wastewater are preferred over alternative treatment methods due to their advantages (Warsinger et al., 2017). The PES membrane coated with MgB_2 nanosheets was investigated to evaluate the microbiological removal performance of both the surface of this membrane and the membrane filtration procedure. As a model bacteria, *E. coli* was used in this study. Obtained results are shown in Figs. 13 and 14. With an increase in the percentage of MgB_2 nanosheets coated on the membrane, both the membrane surface and the membrane filtering process became more effective in antimicrobial ability. The antimicrobial performance of the membrane surface was determined as 96.75 ± 5.91%, 99.57 ± 5.98%, and 99.92 ± 5.3% at 0.5, 1.0, and 2.0% MgB_2 nanosheets concentrations, respectively. The performance of the membrane filtration process was 98.89 ± 5.92%, 99.89 ± 5.86%, and 100 ± 6.05% at 0.5, 1.0, and 2.0% MgB_2 nanosheets concentrations, respectively. These findings suggest that the treatment of water contaminated by microorganisms can be accomplished using PES membranes blended with MgB_2 nanosheets.

4. Conclusions

In this study, MgB_2 nanosheets were produced successfully by ultrasonication of MgB_2 particles in pure water, and MgB_2 nanosheets were characterized. The experimental data demonstrated that MgB_2 nanosheets had considerable biological activities on tests for antioxidant, antimicrobial, DNA nuclease, cell viability inhibition, and antibiofilm activities. Moreover, the pristine and MgB_2 nanosheets blended composite membranes were prepared using the phase inversion method. The pure water flux and BSA flux increased after the blending of MgB_2 nanosheets. On the other hand, BSA removal efficiency increased from 65.5% to 95.5%. Antifouling performance of the composite membranes was also investigated for *E. coli* filtration. A blending of MgB_2 nanosheets improved the anti-fouling properties of pristine PES membranes. The obtained data revealed that it can be used as an alternative method for the treatment of wastewater. In addition, the homogeneous distribution of MgB_2 nanosheets in the structure of PES membranes suggests that they may be a good alternative for many applications such as paint and packaging, where antimicrobial activity is expected in the future.

Credit author statement

Ridvan Kucukosman – concepts, design, data collection and experimentation, Zelal Isik – concepts, design, data collection and

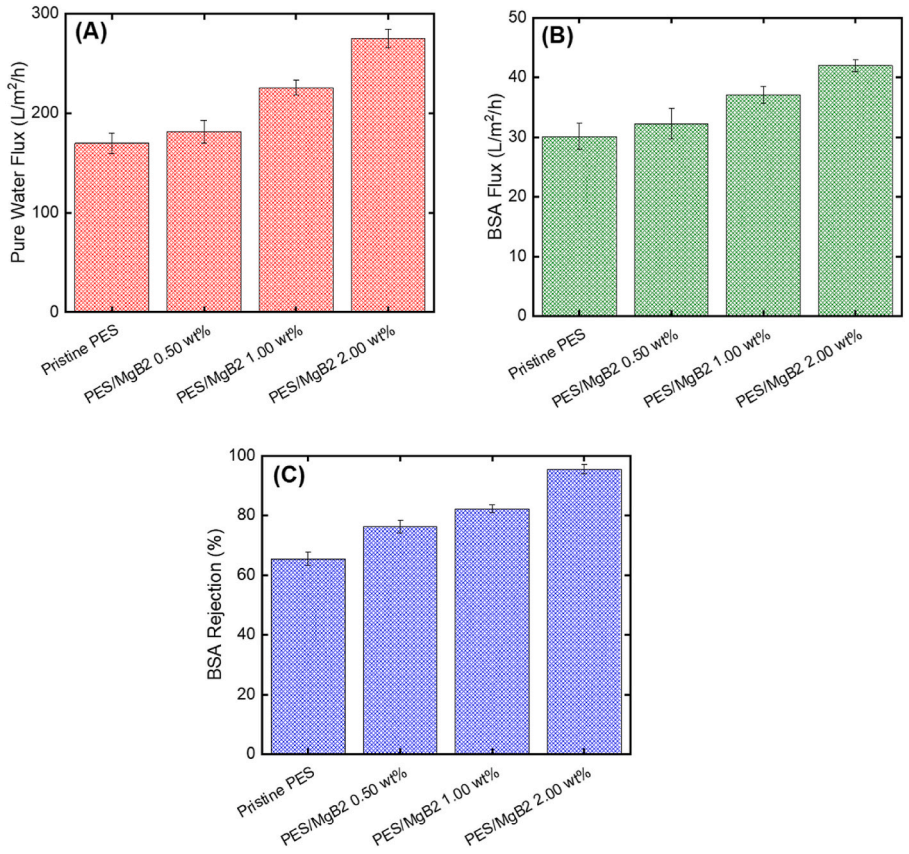

Fig. 11. MgB_2 nanosheets-blended composite PES membrane performance **(A)** PWF, **(B)** BSA flux, and **(C)** BSA rejection.

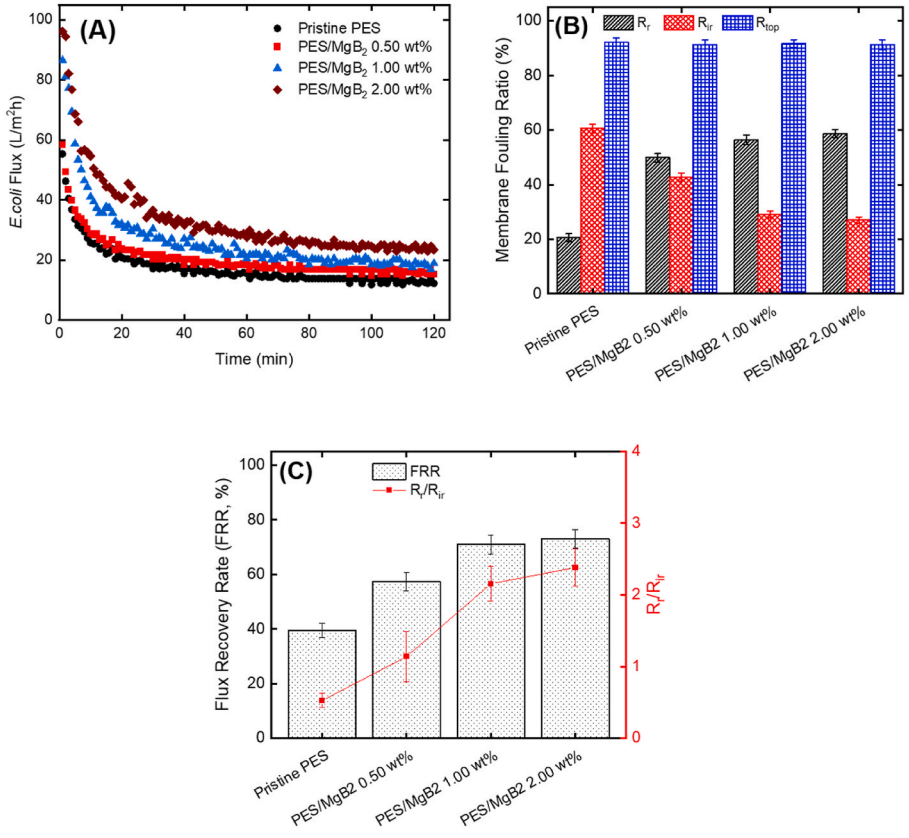

Fig. 12. **(A)** *E. coli* filtration versus time, **(B)** Resistance values of the membranes and **(C)** Flux recovery rate and R_r/R_{ir} ratios of the membranes.

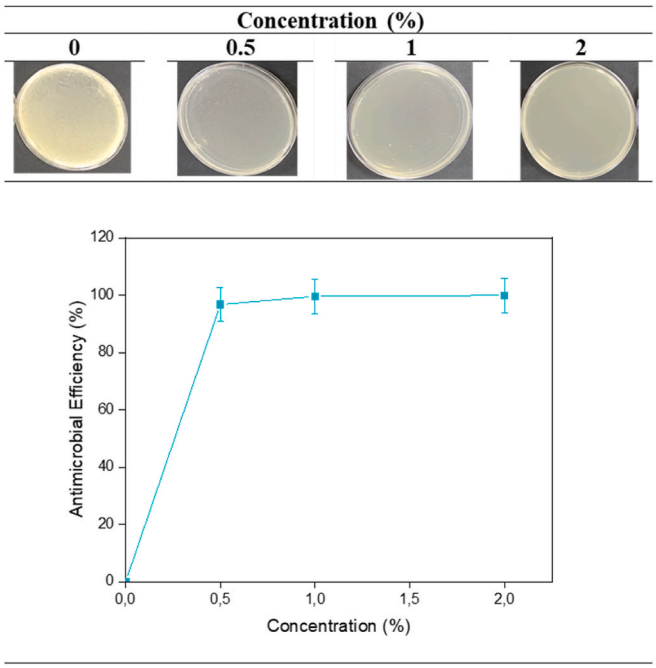

Fig. 13. Performing of PES membrane surface blended with MgB_2 nanosheets for removal of *E. coli*.

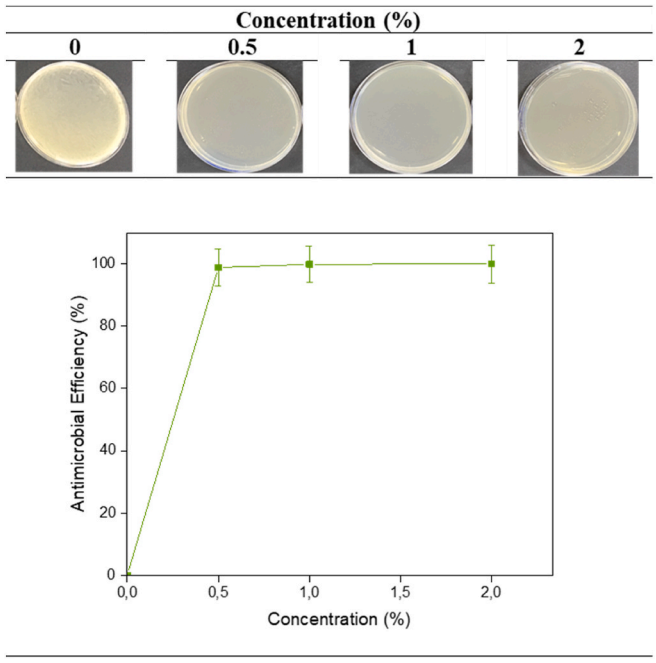

Fig. 14. Performing of PES membrane blended with MgB_2 nanosheets for *E. coli* filtration process.

experimentation, Kasim Ocakoglu – concepts, design, data collection and experimentation, Nadir Dizge – concepts and design, draft, technical correction and proof read, Sadin Özdemir – concepts, design, data collection and experimentation, M. Serkan Yalçın – concepts and design, draft, technical correction and proof read, Prabakar Sharma–draft, technical correction and proof read, Deepanraj Balakrishnan - concepts and design, draft, technical correction and proof read.

Declaration of competing interest

The authors declare that they have no known competing financial interests or personal relationships that could have appeared to influence the work reported in this paper.

Data availability

No data was used for the research described in the article.

References

Bajpai, V.K., Baek, K.H., Kang, S.C., 2017. Antioxidant and free radical scavenging activities of taxoquinone, a diterpenoid isolated from Metasequoia glyptostroboides. South Afr. J. Bot. 111, 93–98. https://doi.org/10.1016/J.SAJB.2017.03.004.

Das, B., Moumita, S., Ghosh, S., Khan, M.I., Indira, D., Jayabalan, R., Tripathy, S.K., Mishra, A., Balasubramanian, P., 2018. Biosynthesis of magnesium oxide (MgO) nanoflakes by using leaf extract of Bauhinia purpurea and evaluation of its antibacterial property against Staphylococcus aureus. Mater. Sci. Eng. C 91, 436–444. https://doi.org/10.1016/J.MSEC.2018.05.059.

Deshmukh, A.R., Aloui, H., Kim, B.S., 2020. In situ growth of gold and silver nanoparticles onto phyto-functionalized boron nitride nanosheets: catalytic, peroxidase mimicking, and antimicrobial activity. J. Clean. Prod. 270, 122339 https://doi.org/10.1016/J.JCLEPRO.2020.122339.

Di Martino, P., 2018. Extracellular polymeric substances, a key element in understanding biofilm phenotype. AIMS Microbiol 4, 274. https://doi.org/10.3934/MICROBIOL.2018.2.274.

Dizaj, S.M., Lotfipour, F., Barzegar-Jalali, M., Zarrintan, M.H., Adibkia, K., 2014. Antimicrobial activity of the metals and metal oxide nanoparticles. Mater. Sci. Eng. C 44, 278–284. https://doi.org/10.1016/J.MSEC.2014.08.031.

Dobrucka, R., 2018. Synthesis of MgO nanoparticles using artemisia abrotanum herba extract and their antioxidant and photocatalytic properties. Iran. J. Sci. Technol. Trans. A Sci. 42, 547–555. https://doi.org/10.1007/S40995-016-0076-X/TABLES/1.

Dutta, R.K., Nenavathu, B.P., Gangishetty, M.K., 2013. Correlation between defects in capped ZnO nanoparticles and their antibacterial activity. J. Photochem. Photobiol. B Biol. 126, 105–111. https://doi.org/10.1016/J.JPHOTOBIOL.2013.07.010.

Efeoğlu, İ., Totık, Y., Keleş, A., Gülten, G., Ersoy, K., Durkaya, G., 2019. The adhesion and tribological properties of c-BN films deposited by high power impulse magnetron sputtering. Ceram. Int. 45, 3000–3006. https://doi.org/10.1016/J.CERAMINT.2018.10.061.

Gunda, H., Das, S.K., Jasuja, K., 2018. Simple, green, and high-yield production of boron-based nanostructures with diverse morphologies by dissolution and recrystallization of layered magnesium diboride crystals in water. ChemPhysChem 19, 880–891. https://doi.org/10.1002/CPHC.201701033.

Iftikhar, M., Noureen, A., Jabeen, F., Uzair, M., Rehman, N., Sher, E.K., Katubi, K.M., Américo-Pinheiro, J.H.P., Sher, F., 2023. Bioinspired engineered nickel nanoparticles with multifunctional attributes for reproductive toxicity. Chemosphere 311, 136927. https://doi.org/10.1016/j.chemosphere.2022.136927. Part 1.

Jasim, N.A., Al-Gasha'a, F.A., Al-Marjani, M.F., Al-Rahal, A.H., Abid, H.A., Al-Kadhmi, N. A., Jakaria, M., Rheima, A.M., 2020. ZnO nanoparticles inhibit growth and biofilm formation of vancomycin-resistant S. aureus (VRSA). Biocatal. Agric. Biotechnol. 29, 101745 https://doi.org/10.1016/J.BCAB.2020.101745.

Jessop, P.G., Ahmadpour, F., Buczynski, M.A., Burns, T.J., Green, N.B., Korwin, R., Long, D., Massad, S.K., Manley, J.B., Omidbakhsh, N., Pearl, R., Pereira, S., Predale, R.A., Sliva, P.G., Vanderbilt, H., Weller, S., Wolf, M.H., 2013. Opportunities for greener alternatives in chemical formulations. J. Name 00, 1. https://doi.org/10.1039/x0xx00000x. –3.

John Sushma, N., Prathyusha, D., Swathi, G., Madhavi, T., Deva Prasad Raju, B., Mallikarjuna, K., Kim, H.S., 2016. Facile approach to synthesize magnesium oxide nanoparticles by using Clitoria ternatea—characterization and in vitro antioxidant studies. Appl. Nanosci. 6, 437–444. https://doi.org/10.1007/S13204-015-0455-1/FIGURES/11.

Khalid, A.D., Ur-Rehman, N., Tariq, G.H., Ullah, S., Buzdar, S.A., Iqbal, S.S., Sher, E.K., Alsaiari, N.S., Hickman, G.J., Sher, F., 2023. Functional bioinspired nanocomposites for anticancer activity with generation of reactive oxygen species. Chemosphere 310, 136885. https://doi.org/10.1016/j.chemosphere.2022.136885.

Khan, N.A., Niazi, M.B.K., Sher, F., Jahan, Z., Noor, T., Azhar, O., Rashid, T., Iqbal, N., 2021. Metal organic frameworks derived sustainable polyvinyl alcohol/starch nanocomposite films as robust materials for packaging applications. Polymers 13, 2307. https://doi.org/10.3390/polym13142307.

Kıvanç, M., Barutca, B., Koparal, A.T., Göncü, Y., Bostancı, S.H., Ay, N., 2018. Effects of hexagonal boron nitride nanoparticles on antimicrobial and antibiofilm activities, cell viability. Mater. Sci. Eng. C 91, 115–124. https://doi.org/10.1016/J.MSEC.2018.05.028.

Krishnamoorthy, K., Veerapandian, M., Zhang, L.H., Yun, K., Kim, S.J., 2012. Antibacterial efficiency of graphene nanosheets against pathogenic bacteria via lipid peroxidation. J. Phys. Chem. C 116, 17280–17287. https://doi.org/10.1021/JP3047054/ASSET/IMAGES/MEDIUM/JP-2012-047054_0008.

Li, X. Bin, Xie, S.Y., Zheng, H., Tian, W.Q., Sun, H.B., 2015. Boron based two-dimensional crystals: theoretical design, realization proposal and applications. Nanoscale 7, 18863–18871. https://doi.org/10.1039/C5NR04359J.

Li, H., Jing, L., Liu, W., Lin, J., Tay, R.Y., Tsang, S.H., Teo, E.H.T., 2018. Scalable production of few-layer boron sheets by liquid-phase exfoliation and their superior supercapacitive performance. ACS Nano 12, 1262–1272. https://doi.org/10.1021/ACSNANO.7B07444/SUPPL_FILE/NN7B07444_SI_001.PDF.

Liang, D., Liu, J., Zhou, Y., Zhou, J., 2017. Ignition and combustion characteristics of amorphous boron and coated boron particles in oxygen jet. Combust. Flame 185, 292–300. https://doi.org/10.1016/J.COMBUSTFLAME.2017.07.030.

Mannix, A.J., Zhou, X.F., Kiraly, B., Wood, J.D., Alducin, D., Myers, B.D., Liu, X., Fisher, B.L., Santiago, U., Guest, J.R., Yacaman, M.J., Ponce, A., Oganov, A.R., Hersam, M.C., Guisinger, N.P., 2015. Synthesis of borophenes: anisotropic, two-dimensional boron polymorphs. Science 350, 1513–1516. https://doi.org/10.1126/SCIENCE.AAD1080.

Mavukkandy, M.O., McBride, S.A., Warsinger, D.M., Dizge, N., Hasan, S.W., Arafat, H.A., 2020. Thin film deposition techniques for polymeric membranes– A review. J. Membr. Sci. 610, 118258 https://doi.org/10.1016/J.MEMSCI.2020.118258.

MubarakAli, D., Manzoor, M.A.P., Sabarinathan, A., Anchana Devi, C., Rekha, P.D., Thajuddin, N., Lee, S.Y., 2019. An investigation of antibiofilm and cytotoxic property of MgO nanoparticles. Biocatal. Agric. Biotechnol. 18, 101069 https://doi.org/10.1016/J.BCAB.2019.101069.

M'barek, I., Isik, Z., Ozay, Y., Özdemir, S., Tollu, G., Moussaoui, Y., Dizge, N., 2022. Nanocellulose synthesis from Tamarix aphylla and preparation of hybrid nanocellulose composites membranes with investigation of antioxidant and antibacterial effects. Separ. Purif. Technol. 292, 120815 https://doi.org/10.1016/j.seppur.2022.120815.

Mubeen, B., Ansar, A.N., Rasool, R., Ullah, I., Imam, S.S., Alshehri, S., Ghoneim, M.M., Alzarea, S.I., Nadeem, M.S., Kazmi, I., 2021. Nanotechnology as a novel approach in combating microbes providing an alternative to antibiotics. Antibiot 2021, 1473. https://doi.org/10.3390/ANTIBIOTICS10121473, 10, Page 1473 10.

Nishino, H., Fujita, T., Yamamoto, A., Fujimori, T., Fujino, A., Ito, S.I., Nakamura, J., Hosono, H., Kondo, T., 2017. Formation mechanism of boron-based nanosheet through the reaction of MgB2 with water. J. Phys. Chem. C 121, 10587–10593. https://doi.org/10.1021/ACS.JPCC.7B02348/SUPPL_FILE/JP7B02348_SI_001.PDF.

Olaolu, D.T., Akpor, O.B., Akor, C.O., 2014. Pollution Indicators and Pathogenic Microorganisms in Wastewater Treatment: Implication on Receiving Water Bodies.

Patel, R.B., Chou, T., Iqbal, Z., 2015. Synthesis of boron nanowires, nanotubes, and nanosheets. J. Nanomater. 2015, 243925 https://doi.org/10.1155/2015/243925.

Pugazhendhi, A., Prabhu, R., Muruganantham, K., Shanmuganathan, R., Natarajan, S., 2019. Anticancer, antimicrobial and photocatalytic activities of green synthesized magnesium oxide nanoparticles (MgONPs) using aqueous extract of Sargassum wightii. J. Photochem. Photobiol. B Biol. 190, 86–97. https://doi.org/10.1016/J.JPHOTOBIOL.2018.11.014.

Russell, B.A., Kubiak-Ossowska, K., Mulheran, P.A., Birch, D.J.S., Chen, Y., 2015. Locating the nucleation sites for protein encapsulated gold nanoclusters: a molecular dynamics and fluorescence study. Phys. Chem. Chem. Phys. 17, 21935–21941. https://doi.org/10.1039/C5CP02380G.

Saleh, M., Gonca, S., Isik, Z., Ozay, Y., Harputlu, E., Ozdemir, S., Yalvac, M., Ocakoglu, K., Dizge, N., 2021. Preparation of ZnO nanorods or SiO2 nanoparticles grafted onto basalt ceramic membrane and the use for E. coli removal from water. Ceram. Int. 47, 27710–27717. https://doi.org/10.1016/J.CERAMINT.2021.06.196.

Scheifers, J.P., Zhang, Y., Fokwa, B.P.T., 2017. Boron: enabling exciting metal-rich structures and magnetic properties. Acc. Chem. Res. 50, 2317–2325. https://doi.org/10.1021/ACS.ACCOUNTS.7B00268/ASSET/IMAGES/MEDIUM/AR-2017-00268S_0008.

Seil, J.T., Webster, T.J., 2012. Antimicrobial applications of nanotechnology: methods and literature. Int. J. Nanomed. 7, 2767–2781. https://doi.org/10.2147/IJN.S24805.

Tai, G., Hu, T., Zhou, Y., Wang, X., Kong, J., Zeng, T., You, Y., Wang, Q., 2015. Synthesis of atomically thin boron films on copper foils. Angew Chem. Int. Ed. Engl. 54, 15473–15477. https://doi.org/10.1002/ANIE.201509285.

Taşaltın, N., Güllülü, S., Karakuş, S., 2022. Dual-role of β borophene nanosheets as highly effective antibacterial and antifungal agent. Inorg. Chem. Commun. 136, 109150 https://doi.org/10.1016/J.INOCHE.2021.109150.

Wang, L., Hu, C., Shao, L., 2017a. The antimicrobial activity of nanoparticles: present situation and prospects for the future. Int. J. Nanomed. 12, 1227. https://doi.org/10.2147/IJN.S121956.

Wang, Y., Li, L., Wei, Y., Xue, j., Chen, H., Ding, L., Caro, J., Wang, H., 2017b. Water transport with ultralow friction through partially exfoliated g-C3N4 nanosheet membranes with self-supporting spacers. Angew. Chem. Int. Ed. 56, 8974–8980. https://doi.org/10.1002/anie.201701288.

Warsinger, D.M., Tow, E.W., Swaminathan, J., Lienhard, V.J.H., 2017. Theoretical framework for predicting inorganic fouling in membrane distillation and experimental validation with calcium sulfate. J. Membr. Sci. 528, 381–390. https://doi.org/10.1016/J.MEMSCI.2017.01.031.

Xu, J., Chang, Y., Gan, Lin, Ma, Ying, Zhai, T., Xu, J.Q., Chang, Y.Y., Gan, L., Ma, Y., Zhai, T.Y., 2015. Ultrathin single-crystalline boron nanosheets for enhanced electro-optical performances. Adv. Sci. 2, 1500023 https://doi.org/10.1002/ADVS.201500023.

Yao, J., Liu, C., Liu, X., Guo, J., Zhang, S., Zheng, J., Li, S., 2020. Azobenzene-assisted exfoliation of 2D covalent organic frameworks into large-area, few-layer nanosheets for high flux and selective molecular separation membrane. J. Membr. Sci. 601, 117864 https://doi.org/10.1016/j.memsci.2020.117864.

Zhang, Z., Yang, Y., Gao, G., Yakobson, B.I., 2015. Two-dimensional boron monolayers mediated by metal substrates. Angew. Chem. Int. Ed. 54, 13022–13026. https://doi.org/10.1002/ANIE.201505425.

Zhang, X., Li, H., Wang, J., Peng, D., Liu, J., Zhang, Y., 2019. In-situ grown covalent organic framework nanosheets on graphene for membrane-based dye/salt separation. J. Membr. Sci. 581, 321–330. https://doi.org/10.1016/j.memsci.2019.03.070.